Proceeding of the 7th International Symposium on Artificial Intelligence, Robotics and Automation in Space:
i-SAIRAS 2003, NARA, Japan, May 19-23, 2003

Evaluation of Uneven Terrain Traversability for Wheeled Mobile Robots by Fractal Terrain Model

Yasuyoshi YOKOKOHJI, Satoshi CHAEN and Tsuneo YOSHIKAWA
Department of Mechanical Engineering, Graduate School of Engineering
Kyoto University, Kyoto 606-8501, Japan
{yokokoji|yoshi}@mech.kyoto-u.ac.jp

Keywords: planetary rover, fractal theory, terrain model, fractional Brownian motion, traversability, mobile robot

Abstract

Planetary rover should be designed so that it can travel on uneven terrains robustly under several limitations such as size, weight, costs, etc. However, it is difficult to get precise or whole terrain information beforehand to check the performance of the designed rover.

In this paper, we propose a simulation model of uneven terrains based on fractional Brownian motions (fBm's) for evaluating traversability of mobile robots. Using fBm model, one can generate various terrain models by changing only two parameters. We modeled two different terrains by using fBm and checked statistical traversability of a robot with different wheel sizes and body configurations in computer simulation. To validate the effectiveness of the fBm model, we conducted real experiments with a wheeled mobile robot. Probabilities that the robot can travel a certain distance well agreed with the simulation results.

The proposed method would be useful to find a guideline for designing planetary rovers and some new rover mechanisms that can travel on uneven terrains robustly.

1 Introduction

Planetary rover should be designed so that it can travel on uneven terrains robustly under several limitations such as size, weight, costs, etc. However, it is almost impossible to design a rover that can traverse a target terrain with 100% probability without getting stuck, because it is difficult to get precise terrain information beforehand and check the performance of the designed rover.

To evaluate traversability of planetary rovers in computer simulation, we need a rover dynamics model, a precise terrain model, and an accurate contact dynamics model between them. Yoshida *et al.*[6] studied a motion dynamics simulation model of rovers on uneven natural terrains. They discussed wheel traction model but modeling of terrains was not considered. Since the roughness of terrains may vary from place to place even on the same planet, traversability should be checked on variety of terrains. Fractal theory shows that fractional Brownian motion (fBm's) can mathematically represent complex shapes in nature, such as coastlines, clouds and mountains[3][4]. Yoshikawa and Nishiguchi[7][8] used fBm to extrapolate an imperfect image of the moon surface to determine the best landing point. To our best knowledge, however, fBm has not been used for terrain modeling to evaluate the traversability of rovers.

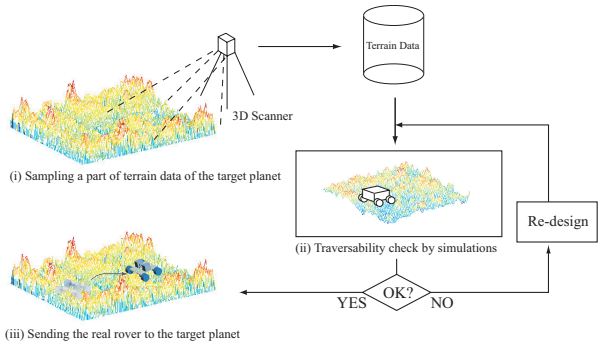

Figure 1: Flow of the proposed method

In this paper, we propose a simulation model of uneven terrains based on fractional Brownian motions (fBm's) for evaluating traversability of mobile robots. Using fBm model, one can generate various terrain models by changing only two parameters. We modeled two different terrains by using fBm and checked statistical traversability of a robot with different wheel sizes and body configurations in computer simulation. To validate the effectiveness of the fBm model, we conducted real experiments with a wheeled mobile robot. Probabilities that the robot can travel a certain distance well agreed with the simulation results.

2 Outline of the proposed method

2.1 Designing a robust rover

Developing a rover and sending it to a target planet need a lot of costs. Therefore, planet rovers must have high

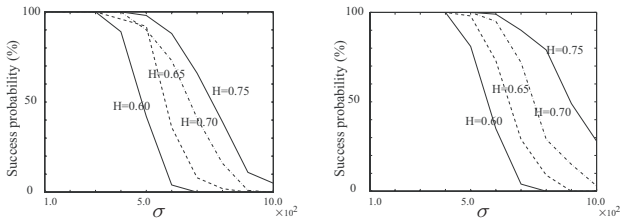

(a) Diameter 60[cm] (b) Diameter 100[cm]

Figure 2: Preliminary results with 2-D simulation

traversability on the terrain of the target planet in order to make the mission successful. However, it is impossible to check the traversability in advance on the target planet. In such a situation, we propose to use a terrain model using fBm.

Figure 1 illustrates a flow of the proposed method. We assume that partial terrain data can be obtained from, for example, a satellite orbiting the target planet. Instead of using this real terrain data, we make an fBm terrain model that approximates this real terrain. Using fBm terrain models, we can evaluate the traversability of the designed rover many times in computer simulation and redesign the rover if necessary. After we make sure that the designed rover can traverse the terrain robustly, we can actually send the rover to the target planet.

2.2 Why not real terrain data?

One might argue that why we do not use the real terrain data. As shown in the following section, fBm model can represent various terrains by only two parameters. As mentioned above, it is impossible to obtain whole terrain data in advance. Checking only on the partial terrain data might not be enough to ensure the robust traversability. On the other hand, the fBm model can generate a variety of terrains by introducing random numbers. To make the rover robust, we might also want to check the traversability on a terrain that is a little rougher than the real one. It is easy to make such a terrain model by changing the parameters.

Figure 2 shows the simulation results of our preliminary research using 2-dimentional terrain models[5]. We tested two different wheel diameters on various terrain models by changing two parameters, σ and H. One can see that the success rate to traverse a certain distance becomes low when increasing σ or decreasing H, and larger wheel shows higher traversability. From this kind of simulation studies, one can design a rover that is statically guaranteed to traverse the target terrain under the size and weight constraints.

3 Terrain Modeling by fBm

3.1 Fractional Brownian motion (fBm)

Fractional Brownian motion (fBm) is one of the most effective mathematical models for representing natural terrains such as Mars and a mountain range[3]. The fBm can be represented as a random function of time, $V(t)$, which spectrum density $S(f)$ is given by

$$S(f) = \frac{\sigma^2}{f^{2H+1}}, \tag{1}$$

where f denotes frequency, σ is the standard deviation of the Gaussian distribution, and H ($0 < H < 1$) is called Hurst Parameter. Parameter H determines the characteristic of undulation and σ determines the amplitude of undulation.

The spectrum approximation method is a method to generate a random function that agrees with the required spectrum density based on eq.(1). Suppose that the goal fBm can be decomposed to N finite sequence of numbers, V_k. By using discrete Fourier transformation, V_k can be given by

$$V_k = \frac{1}{N} \sum_{j=0}^{N-1} v_j e^{2\pi i f_j t_k}, \tag{2}$$

where v_j denotes complex Fourier coefficients.

Therefore, if we want to make a sequence of numbers of fBm which spectrum density is given by eq.(1), each coefficient v_j must satisfy the following equation:

$$E(|v_j|^2) = \frac{\sigma^2}{f_j^{2H+1}}, \tag{3}$$

where $E(\cdot)$ denotes expectation value. Once the coefficient v_j that satisfies eq.(3) is selected, the goal fBm sequence can be obtained by using discrete inverse Fourier transformation.

3.2 Modeling of 3D terrains

Although fBm is originally a function of time $V(t)$, it is possible to use fBm for modeling 3D terrains by extending it to a function with two variables. Suppose that the height of 3D terrains is given by a function of two dimensional horizontal position as $Z = Z(x, y)$. If this $Z(x, y)$ has the statistical characteristic of fBm, it can model the natural 3D terrains.

Let $S(u, v)$ be the spectral density function of $Z(x, y)$, where (u, y) denotes spatial frequencies corresponding to (x, y). Extending eq.(1), $S(u, v)$ must satisfy the following equation[3]:

$$S(u, v) = \frac{\sigma^2}{(u^2 + v^2)^{H+1}}. \tag{4}$$

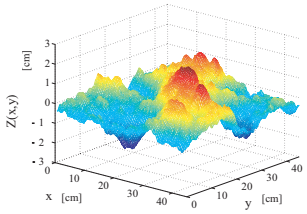

Figure 3: 3D uneven terrain model by fBm

Suppose that $Z(x, y)$ can be decomposed to $N \times N$ finite sequence of numbers, $Z(x_j, y_k)$ $(x_j, y_k = 0, 1/N, 2/N, \cdots, (N-1)/N)$. Then it can be given by

$$Z(x_j, y_k) = \frac{1}{N^2} \sum_{l=0}^{N-1} \sum_{m=0}^{N-1} z_{lm} e^{2\pi i (u_l x_j + v_m y_k)}. \quad (5)$$

To model the 3D uneven terrains, we can set a random function z_{jk} that satisfies the following equation:

$$E(|z_{jk}|^2) = \frac{\sigma^2}{(u_j^2 + v_k^2)^{H+1}}. \quad (6)$$

Once the coefficient z_{jk} is determined, $Z(x, y)$ can be obtained by discrete inverse Fourier transformation.

Similarly to the previous case, two parameters, H and σ, determine the characteristic of the terrain. Figure 3 shows an example of terrain model using fBm.

3.3 Parameter identification from real terrain data

As we mentioned in the previous section, we use fBm terrain models that approximate the real target terrain in order to check the traversability of the rover in computer simulation. To construct a fBm model that represents the real terrain, we need to identify the parameters H and σ.

Taking logarithm of both sides of eq.(4), we get

$$\log_{10} S(u, v) = \log_{10} \sigma^2 - (H+1) \log_{10}(u^2 + v^2). \quad (7)$$

Namely, when we plot $S(u, v)$ and $(u^2 + v^2)$ of a fBm model on a log-log graph, we have a line with inclination of $-(H+1)$ and intercept of $\log_{10} \sigma^2$. Therefore, to identify the parameters, we first plot the power spectrum densities of the target terrain on a log-log graph as shown in Fig.4. Then, we get a regression line from these plots and estimate H and σ from the inclination and intercept of this regression line.

Power spectrum density of the real terrain can be obtained from the Fourier coefficients of the terrain data as

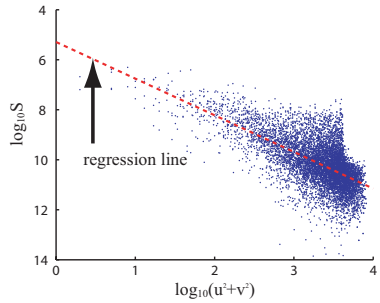

Figure 4: Parameter estimation from the real terrain data

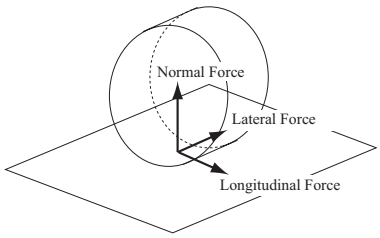

Figure 5: Three components of the reaction force

follows:

$$S(u, v) = \frac{1}{N^4} \{ |z_{j,k}|^2 + |z_{N-j,N-k}|^2 + |z_{j,N-k}|^2 + |z_{N-j,k}|^2 \} \quad (j, k = 0, 1, 2, \cdots, \frac{N}{2}). \quad (8)$$

4 Dynamics of Wheeled Mobile Robots

4.1 Contact dynamics of wheels and terrains

It is very important to analyze contact dynamics between wheels and the terrain in order to obtain precise simulation results.

Contact dynamics on uneven terrains is more complex than that for flat terrains. In this section, we will extend the method by Gim and Nikravesh[1] to the uneven terrain case. First, we assume that the wheel shape is column. Next, we decompose the reaction force from the ground into three components, longitudinal force, lateral force and

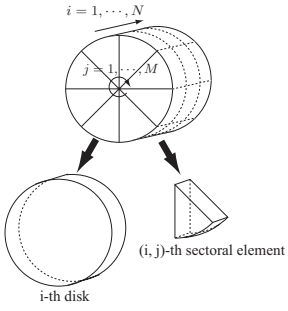

Figure 6: Dividing the wheel into small elements

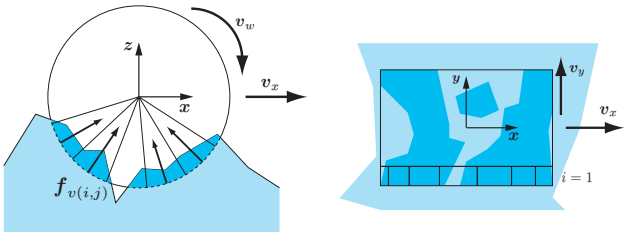

(a) Side view (b) Top view

Figure 7: Calculation of the contact normal force

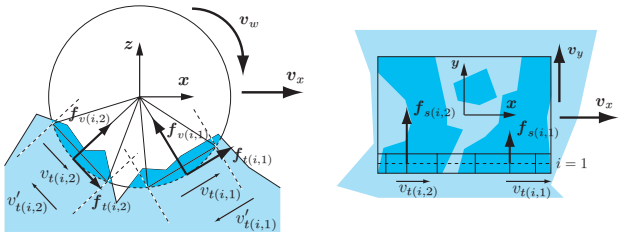

(a) Longitudinal force (b) Lateral force

Figure 8: Calculation of the longitudinal and lateral forces

contact normal force, as shown in Fig.5. To calculate reaction forces, we will divide the wheel into small elements as shown in Fig.6. Each wheel is first divided into N disks to calculate longitudinal and lateral forces. Then, each disk is divided into M sectoral elements to calculate contact normal forces.

Calculating contact normal force

In this paper, we assume that the wheel is elastic and it is deformed when it comes in contact with the terrain. Contact normal force is calculated from the penetration area of the wheel into the terrain. Although contact normal can be obtained uniquely on a flat surface, it is difficult to obtain the contact normal on an uneven terrain. To calculate the contact normal force, we first calculate the contact force from each sectoral element as shown in Fig.7.

Let V_{ij} be the penetration volume of (i,j)-th sectoral element. Letting R be the radius of the wheel and $R_{m(i,j)}$ be the averaged distance from the wheel axis to the terrain surface within the (i,j)-th element, V_{ij} is given by

$$V_{ij} = \frac{1}{2}(R^2 - R_{m(i,j)}^2)\phi d, \tag{9}$$

where ϕ denotes the central angle of the sectoral element and d means the width of the element. Then, the amount of wheel deformation h_{ij} is given by

$$h_{ij} = \frac{V_{ij}}{R\phi d}. \tag{10}$$

The contact normal force at (i,j)-th sectoral element, $\boldsymbol{f}_{v(ij)}$, is obtained from the following equation:

$$\boldsymbol{f}_{v(i,j)} = (K_v h_{ij} + D_v \dot{h}_{ij})\boldsymbol{e}_{ij}, \tag{11}$$

where K_v and D_v are stiffness and viscosity parameters of the wheel, respectively, and $\boldsymbol{e}_{ij}$ denotes the unit vector directing from the contact surface of (i,j)-th sectoral element to the wheel axis.

Calculating longitudinal and lateral forces

To calculate longitudinal and lateral forces, we extend the method by Gim and Nikravesh[1] to the uneven terrain case. Here, each wheel is divided in to thin disks and longitudinal and lateral forces are calculated on each disk.

Unlike the flat surface case, the wheel may have multiple contact sections when contacting with uneven terrains as shown in Fig.8(a). Let N_i be the number of these contact sections of i-th disk. We apply the method by Gim and Nikravesh[1] to each section, and then calculate the total forces by summing the contributions from all disks. The detail of the method is described as follows.

STEP 1

Let $v_{t(i,k)}$ be the tangential component of the vehicle velocity at k-th contact section of i-th disk, and let v_y be the lateral component of the vehicle velocity. Letting $v'_{t(i,k)} = -v_{t(i,k)}$ be the reverse velocity, slip ratio $S_{t(i,k)}$ and lateral slip ratio $S_{\alpha(i,k)}$ at k-th contact section of i-th disk can be obtained by

$$S_{t(i,k)} = \begin{cases} (v'_{t(i,k)} - v_w)/v'_{t(i,k)} & (v'_{t(i,k)} > v_w) \\ (v'_{t(i,k)} - v_w)/v_w & (v'_{t(i,k)} < v_w) \end{cases} \tag{12}$$

and

$$S_{\alpha(i,k)} = \begin{cases} |\tan\alpha_{(i,k)}| & (v_{t(i,k)} > v_w) \\ (1 - |S_{t(i,k)}|)|\tan\alpha_{(i,k)}| & (v_{t(i,k)} < v_w) \end{cases} \tag{13}$$

where $v_w = R\omega$ denotes tangential velocity of the wheel due to the wheel rotation ω and $\alpha_{(i,k)} = \tan^{-1}(v_y/v_{t(i,k)})$ means the slip angle at k-th contact section of i-th disk.

STEP 2

From the contact normal force at k-th contact section of i-th disk, $f_{v(i,k)} = |\boldsymbol{f}_{v(i,k)}|$, critical slip ratio $S^*_{t(i,k)}$ and critical lateral slip ratio $S^*_{\alpha(i,k)}$ can be obtained by the following equations:

$$S^*_{t(i,k)} = 3\mu_x \frac{f_{v(i,k)}}{C_t}, \tag{14}$$

$$S^*_{\alpha(i,k)} = 3\mu_y \frac{f_{v(i,k)}}{C_\alpha}, \tag{15}$$

where μ_x and μ_y are longitudinal and lateral friction coefficients, and C_t and C_α denote wheel stiffness against longitudinal and lateral deformations, respectively.

Then, adhesion ratios in longitudinal and lateral directions at k-th contact section, $l_{n_t(i,k)}$ and $l_{n_\alpha(i,k)}$, can be obtained by the following equations:

$$l_{n_t(i,k)} = 1 - \frac{|S_{t(i,k)}|}{S^*_{t(i,k)}}, \tag{16}$$

$$l_{n_\alpha(i,k)} = 1 - \frac{|S_{\alpha(i,k)}|}{S^*_{\alpha(i,k)}}. \tag{17}$$

STEP 3
Finally, longitudinal and lateral forces at k-th contact section can be obtained by the following equations:

$$f_{t(i,k)} = \begin{cases} C_t|S_{t(i,k)}|l^2_{n_t(i,k)} + \mu_x f_{v(i,k)}(1 - 3l^2_{n_t(i,k)} \\ \quad + 2l^3_{n_t(i,k)}) & (l_{n_t(i,k)} > 0), \\ \mu_x f_{v(i,k)} & (l_{n_t(i,k)} = 0), \end{cases} \tag{18}$$

$$f_{\alpha(i,k)} = \begin{cases} C_\alpha|S_{\alpha(i,k)}|l^2_{n_\alpha(i,k)} + \mu_y f_{v(i,k)}(1 - 3l^2_{n_\alpha(i,k)} \\ \quad + 2l^3_{n_\alpha(i,k)}) & (l_{n_\alpha(i,k)} > 0), \\ \mu_y f_{v(i,k)} & (l_{n_\alpha(i,k)} = 0). \end{cases} \tag{19}$$

STEP 4
We iterate the calculations of eqs.(18) and (19) for all k $(k = 1, \cdots, N_i)$ of i-th disk and iterate them for all disks $(i = 1, \cdots, N)$. Summing the all contributions up, we get the total longitudinal and lateral forces.

4.2 Contact dynamics of rover body and terrains

On an uneven terrain, the rover body may contact with the terrain. Here, we show the way of calculating reaction forces applying to the rover body from the terrain when the rover body is colliding with the terrain.

Reaction forces have three directions, i.e. vertical (z-direction), longitudinal (x-direction), and lateral (y-direction) direction. Here, we will consider only vertical and longitudinal components and neglect lateral one. Similarly to calculating contact normal forces at the wheel, we divide the body into small columns and calculate the penetration volume in each column. As shown in Fig.9(a), the body is divided vertically along with z-axis to get the vertical component, while it is divided horizontally along with x-axis to get the longitudinal component as shown in Fig.9(b).

Letting $L_{m_v(i)}$ and $L_{m_l(j)}$ $(l = R(\text{right}) \text{ or } L(\text{left}))$ be the averaged penetration depth of i-th vertical column and j-th longitudinal column, respectively, the reaction force on each column can be obtained by

$$\boldsymbol{f}_{bv(i)} = (K_{bv} L_{m_v(i)} + D_{bv} \dot{L}_{m_v(i)}) \boldsymbol{e}_{bv(i)}, \tag{20}$$

$$\boldsymbol{f}_{bl(j)} = (K_{bl} L_{m_l(j)} + D_{bl} \dot{L}_{m_l(j)}) \boldsymbol{e}_{bl(j)}, \tag{21}$$

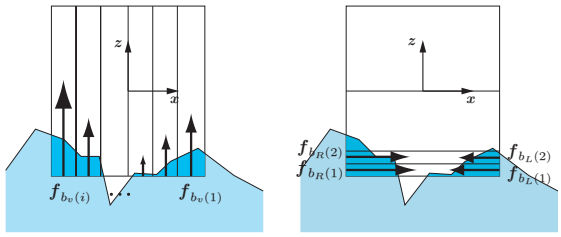

(a) Vertical forces (b) Longitudinal forces

Figure 9: Calculation of the reaction forces applying to the body

where K_{bv} and K_{bl} denote body stiffness in vertical and longitudinal directions, respectively, and D_{bv} and D_{bl} are viscous coefficients. Vectors $\boldsymbol{e}_{bv(i)}$ and $\boldsymbol{e}_{bl(i)}$ are unit vectors along with the column direction. By summing the all contributions up, total reaction force can be obtained.

We also consider friction forces between the body and the terrain as well, assuming dynamic Column friction. Letting $f_{bv(i)} = |\boldsymbol{f}_{bv(i)}|$, friction force acting on i-th vertical column is given by

$$\boldsymbol{f}_{bt(i)} = \mu_{bt} f_{bv(i)} \boldsymbol{e}_{t(i)}, \tag{22}$$

where μ_{bt} denotes dynamic friction coefficient between the vertical column and the terrain, and $\boldsymbol{e}_{t(i)}$ means the unit vector along with the slip direction.

4.3 Equation of motion of the rover

Some rovers have body joints to increase the traversability. Equation of motion of such rovers can be described as follows:

$$\boldsymbol{M} \begin{bmatrix} \ddot{\boldsymbol{p}}_B \\ \dot{\boldsymbol{\omega}}_B \\ \ddot{\boldsymbol{\phi}} \\ \ddot{\boldsymbol{\theta}} \end{bmatrix} + \boldsymbol{h} = \begin{bmatrix} \boldsymbol{f}_B \\ \boldsymbol{n}_B \\ \boldsymbol{n} \\ \boldsymbol{\tau} \end{bmatrix} + \boldsymbol{J}^T \boldsymbol{f}, \tag{23}$$

where $\boldsymbol{M}$ denotes inertia matrix, $\boldsymbol{p}_B$ denotes body position, $\boldsymbol{\omega}_B$ is body angular velocity, $\boldsymbol{\phi}$ is body joint angle, $\boldsymbol{\theta}$ represents wheel rotation angle, $\boldsymbol{h}$ denotes Coriolis and centrifugal forces and gravity force term, $\boldsymbol{f}_B$ and $\boldsymbol{n}_B$ mean total force and moment acting on the body, respectively, $\boldsymbol{n}$ denotes moment acting on the body joint, $\boldsymbol{\tau}$ is wheel driving torque, $\boldsymbol{J}$ is Jacobian matrix, and $\boldsymbol{f}$ means total force and moment acting of the wheels from the terrain.

5 Simulation and Experiment

5.1 Purpose of simulation and experiment

To evaluate the traversability of rovers in computer simulation, simulation results should well agree with the real experiment. There are mainly two factors to determine the simulation accuracy, i.e. terrain model and contact dynamics model. In the previous sections, we have introduced

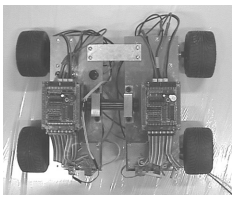
(a) Top view

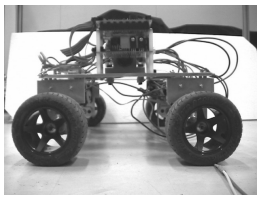
(b) Side view

Figure 10: Rover with large wheels ($D = 90$[mm])

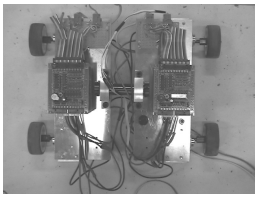
(a) Top view

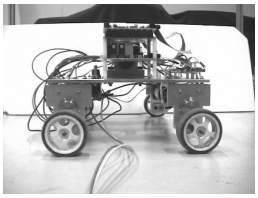
(b) Side view

Figure 11: Rover with small wheels ($D = 60$[mm])

the fBm model of terrain and the contact dynamics modeling. To validate the proposed method, we evaluate the traversability of a rover in computer simulation on two different terrains that have been actually set up in our laboratory. Then, we conducted real experiments to check the actual traversability of the rover on these terrains.

5.2 Rover and terrains

5.2.1 Rover

Figures 10 and 11 show the overview of the rover used in the experiment. The rover has four wheels each of which can be driven by a DC motor independently. Two 8086 compatible CPU boards, two interface boards and two PWM driver boards are mounted on the rover, and CPU boards control the wheels. Two different size of wheels, 90[mm] (Fig.10) or 60[mm] (Fig.11) diameter, can be attached to the rover. The wheels, which are originally for radio control toy vehicles, have rubber tires.

The rover body has two parts connected by a free joint supported by ball bearings. This free joint motion can be disabled by attaching an aluminum plate to the body (Fig.10) or enabled by removing it (Fig.11). Figure 12 shows a CAD model of the rover used in the computer simulation, which well illustrates the configuration of the rover. The body size is roughly 250[mm]×250[mm]. The distance between the wheel axis center and the bottom

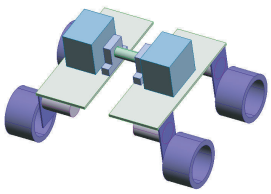

Figure 12: Rover model used in simulation


(a) Gravel terrain

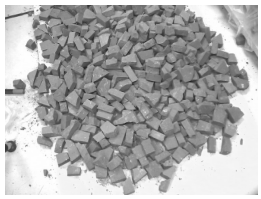
(b) Chopped brick terrain

Figure 13: Two terrains used in the experiment

Figure 14: Size comparison between wheels and terrain components

of the gear unit, which may collide with the terrain, is 15[mm]. Therefore, the road clearance becomes 60[mm] with the large wheel and 45[mm] with the small wheel.

5.2.2 Terrains

We prepared two different terrains in our laboratory. One of them is gravel terrain and the other is chopped brick terrain as shown in Fig.13. Terrain area is approximately 1[m]×1[m] for both terrains. The size of gravel is approximately 1 to 3[cm], and the chopped bricks are sized 5 to 10[cm]. Figure 14 shows two pieces of the gravel and a piece of the chopped brick together with the two wheels to compare these sizes.

5.2.3 Terrain parameter identification

We captured terrain surface profile by a laser range finder (TDS-3100 by Pulstec Industrial Co.,LTD) and identified fBm parameters by plotting the power spectrum densities of the captured surface data. Figures 15 and 16 show the profile of the scanned surface and plots of the power spectrum densities with the regression line. Table 1 shows the identified fBm parameters.

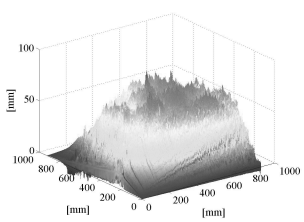

(a) Scanned data

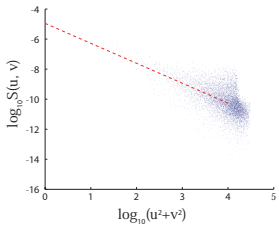

(b) Power spectrum densities

Figure 15: Gravel terrain data

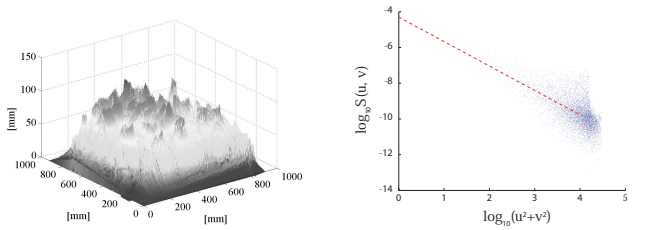

(a) Scanned data (b) Power spectrum densities

Figure 16: Chopped brick terrain data

Table 1: Identified fBm parameters

	H	σ
Gravel	0.33	0.0035
Chopped brick	0.36	0.0080

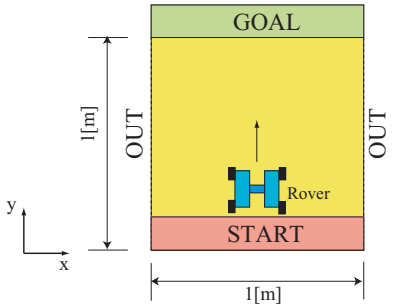

Figure 17: Setup of the simulation

Table 2: Parameters used in the simulation

(a) Body parameters

Mass of center joint&link [kg]	0.23
Mass of body (each half) [kg]	1.8
Gain K_p [Nms/rad]	0.0020
Desired velocity ω_d [rad/s]	3.0
Vertical body stiffness K_{bv} [N/m]	1200
Vertical body viscosity D_{bv} [Ns/m]	200
Longitudinal body stiffness K_{bl} [N/m]	500
Longitudinal body viscosity D_{bl} [Ns/m]	50
Dynamic friction coefficient μ_{bt}	0.4

(b) Wheel parameters

Wheel diameter [mm]	60	90
Wheel mass [kg]	0.03	0.1
Wheel width [mm]	25	55
Radial wheel stiffness K_v [N/m]	5000	3000
Radial wheel viscosity D_v [Ns/m]	200	200
Longitudinal wheel stiffness C_t [N/slip]	150	50
Lateral wheel stifness C_α [N/rad]	500	500
Longitudinal friction coefficient μ_x	0.6	0.9
Lateral friction coefficient μ_y	0.8	1.2

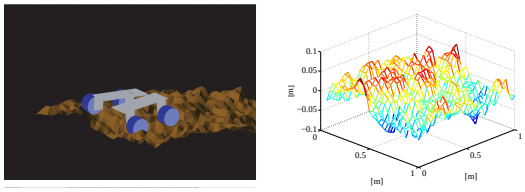

(a) Simulation (b) fBm terrain model

Figure 18: Simulation example (free body joint with large wheels on chopped brick terrain)

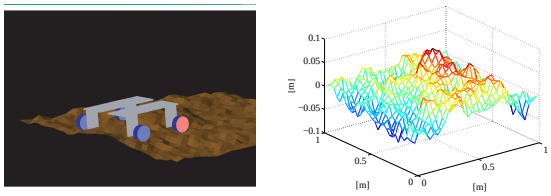

(a) Simulation (b) fBm terrain model

Figure 19: Simulation example (fixed body joint with small wheels on gravel terrain)

5.3 Simulation

Using the identified parameters, we made fBm terrain models and simulate the traversability of the rover. Corresponding to the real rover, each wheel is controlled by the following scheme:

$$\tau_i = K_p(\omega_d - \omega_i) \quad (i = 1 \cdots 4), \tag{24}$$

where τ_i denotes the joint torque of i-th wheel and ω_i denotes angular velocity of i-th wheel. ω_d means the desired angular velocity. Sampling time for direct dynamics computation is 0.5[ms] and motor control sampling time is 3[ms], which also corresponds to the real rover.

Figure 17 illustrates the setup of the simulation. The rover starts from the starting area heading towards the goal area. The terrain area is 1[m]×1[m] and the rover can go anywhere inside this terrain area until reaching the goal. However, if the rover goes out of this terrain area (OUT area) or gets stuck at certain location for more than one second, this trial is judged as failure.

We simulated with two terrains (gravel and chopped brick), two wheel sizes (60[mm] and 90[mm]) and two body configurations (free body joint and fixed body joint), resulting with eight combinations in total, 30 times for each. Table 2 shows the parameters used in the simulation. We consulted [2] to determine some of the wheel parameters. Figures 18 and 19 show some examples of the simulation. Table 3 shows the result of simulation.

5.4 Experiment

Using the real terrains and the real rover, we conducted real experiments with the same eight combinations, 30

Table 3: Success rate in simulation

	Chopped brick	Gravel
D=90[mm], FREE	90%	100%
D=90[mm], FIXED	68%	100%
D=60[mm], FREE	13%	80%
D=60[mm], FIXED	12%	91%

Figure 20: Snapshot of the experiment

times for each, corresponding to the simulation. Figure 20 shows a snapshot of the experiment. Table 4 show the success rate in the experiment.

5.5 Discussion

Compared with the result of simulation and that of experiment, we can say that tendencies are well matched. For example, larger wheel and free body joint show better traversability than smaller wheel and fixed joint, matching to our expectations. However, when the rover had the small wheels (30[mm]), the body joint could not increase the traversability, because the main reason to get stuck was the collision of the body with the terrain.

Mismatch between simulation and experiment results is more evident when the small wheel was used on the gravel terrain. Main reason would be the imprecise modeling of body collisions. In the simulation, we assumed a rigid terrain surface and the rover easily gets stuck when its body collides with the terrain. However, the real gravel terrain is easily deformed after the rover passes through or when the rover body collides with it. Therefore, the rover can often traverse the terrain in the experiment, even if the body collides with the terrain. Deformation model of terrain is one of the future works. Precise modeling of surface property such as friction is also necessary.

Please note that modeling these aspects is necessary anyway even if we do not use the fBm terrain model. We believe that fBm model would become more effective when these aspects can be modeled more precisely.

Table 4: Success rate in experiment

	Chopped brick	Gravel
D=90[mm], FREE	93%	100%
D=90[mm], FIXED	62%	100%
D=60[mm], FREE	0%	100%
D=60[mm], FIXED	0%	85%

6 Conclusion

In this paper, we proposed a simulation model of uneven terrains based on fractional Brownian motions for evaluating traversability of mobile robots. The proposed simulation framework could be helpful for designing a planet rover that can robustly traverse on a target terrain. The proposed model would also be helpful to compare the traversability of various types of vehicles (such as wheeled or caterpillar) on various types of terrains and to invent a novel mobile mechanism.

References

[1] G. Gim and P.E. Nikravesh: “An analytical model of pneumatic tires for vehicle dynamic simulations. Part 1,” Int. J. of Vehicle Design, vol.11, no.6, pp.589-618, 1990.

[2] G. Gim and P.E. Nikravesh: “An analytical model of pneumatic tires for vehicle dynamic simulations. Part 3,” Int. J. of Vehicle Design, vol.12, no.2 pp.217-228, 1991.

[3] B. Mandelbrot: “The Fractal Geometry of Nature,” Henry Holt & Co, 1982.

[4] H-.O. Peitgen and D. Saupe: “The Science of Fractal Images,” Springer Verlag, 1988.

[5] Y. Yokokohji, S. Chaen and T. Yoshikawa: “Modeling of Uneven Terrain by Fractal Theory and Simulation of Wheeled Mobile Robot Motion,” Proc. of the 19th Annual Conference of the Robotics Society of Japan, September 18-20, Tokyo, pp.1309–1310, 2001. (*in Japanese*)

[6] K. Yoshida, H. Asai, and H. Hamano: “Motion Dynamic Simulators and Experiments of an Exploration Rover on Natural Terrain,” Proc. of the 6th International Symposium on Artificial Intelligence and Robotics & Automation in Space (i-SAIRAS 2001), Quebec, Canada, June 18-22, 2001.

[7] S. Yoshikawa and K. Nishiguchi: “Digital elevation map of the moon extrapolated by fractal modeling in the high frequency domain,” 22nd International Symposium on Space Technology and Science, Morioka, Japan, 2000.

[8] S. Yoshikawa and K. Nishiguchi: “Fractal Dimension Estimation and its Application to Constructing a Moon Surface Georama,” Stochastic Systems Symposium, 2000.